Communication

Barriers to Superfast Water Transport in Carbon Nanotube Membranes

Jens Honore Walther, Konstantinos Ritos, Eduardo Cruz-Chu, Constantine M Megaridis, and Petros Koumoutsakos

Nano Lett., **Just Accepted Manuscript** • DOI: 10.1021/nl304000k • Publication Date (Web): 22 Mar 2013

Barriers to Superfast Water Transport in Carbon Nanotube Membranes

Jens H. Walther,[†,§] Konstantinos Ritos,[‡] Eduardo R. Cruz-Chu,[†]

Constantine M. Megaridis,[¶] and Petros Koumoutsakos[*,†]

Computational Science and Engineering Laboratory, ETH Zurich, CH-8092, Switzerland, Department of Mechanical & Aerospace Engineering, University of Strathclyde, Glasgow, G1 1XJ, UK, and Department of Mechanical & Industrial Engineering, University of Illinois at Chicago, Chicago, Illinois 60607, USA

E-mail: petros@ethz.ch

KEYWORDS: Carbon Nanotubes, super fast water transport, Molecular Dynamics

Abstract

Carbon Nanotube (CNT) membranes hold the promise of extraordinary fast water transport for applications such as energy efficient filtration and molecular level drug delivery. However, experiments and computations have reported flow rate enhancements over continuum hydrodynamics, that contradict each other by orders of magnitude. We perform large scale Molecular Dynamics simulations emulating, for the first time, the micrometer thick CNTs membranes used in experiments. We find transport enhancement rates that are length dependent, due to entrance and exit losses, but asymptote to two orders of magnitude over the continuum predictions. These rates are far below those reported experimentally. The results suggest that

[*]To whom correspondence should be addressed
[†]ETH Zurich
[‡]University of Strathclyde
[¶]University of Illinois at Chicago
[§]Department of Mechanical Engineering, Technical University of Denmark, DK-2800 Kgs. Lyngby, Denmark

the reported superfast water transport rates cannot be attributed to interactions of water with pristine CNTs alone.

Water transport through nanoscale pores is of fundamental importance to many natural systems, such as biological ion channels and zeolites, and affects numerous technologies, including molecular level drug delivery, energy efficient nanofiltration and chemical detection. In the last decade, experimental studies provided evidence for superfast water transport through nanometer-wide Carbon Nanotubes (CNTs) embedded in micrometer-thick membranes. Majumder et al.[1,2] reported an enhancement of 4 to 5 orders of magnitude, while Holt et al.[3] found water flow rates that were 2 to 4 orders of magnitude higher than those predicted by corresponding macroscopic, continuum models. On the other hand, more recent experimental results[4] on individual ultralong (several μm) CNTs with diameters in the range 0.81–1.59 nm reported flow enhancement rates below 1000, thus contradicting, for the same diameter, the results of the previous experimental studies.

Contradicting evidence for fast water transport has also been reported for MD simulations. The preponderance of such simulations has been performed either on relatively short (sub 20 nm) nanotubes[5–12] or in periodic domains.[13–15] Thomas and McGaughey[16] considered long ($L = 75$ nm and 150 nm) CNTs connecting two water reservoirs. They found that the measured flow rate is non-linear in the applied pressure gradient, and proposed a modified Darcy law to account for the entrance and exit losses. Contradicting these results, MD simulations[14] in periodic domains and for relatively short times, have reported flow rates that support the experimental findings of super fast transport,[1,3] arguing for reduced friction of water inside the CNT attributed to molecular events. Nevertheless several MD simulations in periodic domains demonstrate flow enhancement rates that are 2–3 orders of magnitude lower[9,13,15] than the experimental measurements.

MD simulations are susceptive on their predictions on initial and boundary conditions.[17,18] Furthermore MD simulations in periodic domains do not account for end-effects induced at the CNT entrance and exit. The importance of these effects in water transport in CNTs has been highlighted in[19] and references therein. A recent MD study[11] has identified length effects of

pressure-driven water transport in sub-10 nm CNTs, and reported enhancement ratios of only up to one order of magnitude above the experimental values. We note that, to the best of our knowledge, MD simulations for experimentally relevant μm thick CNT membranes have never been reported before this study.

Sisan and Lichter[19] examined the importance of entrance and exit losses in CNT flow. Their analysis was based on continuum assumptions and provides a theoretical continuum limit to flow rates in nanochannels. They attributed previous measurements of flow rates above that theoretical limit to possible difficulties in accurately determining channel radii, net flow rates, or the number of channels spanning the membrane. A number of studies[20–24] have examined effective boundary conditions for continuum descriptions of flows in nanopores.

Here, we present large-scale MD simulations of water in CNTs that model the experimental setup of Holt et al.[3] We employ more than 4×10^6 atoms to perform unprecedented large scale MD simulations studying water flow in μm long CNTs thus replicating the lengths used in the experiments. As shown later, these large scale simulations allow us to identify a, previously unexplored, dependence of the transport enhancement rate over a wide range of membrane thicknesses. Furthermore, we examine at an atomistic level the conditions necessary for water to enter, fill and exit the CNTs, as well as the role of the hydrophobicity of the membrane matrix. Previous MD simulations in *periodic* domains have identified the role of the CNT diameter[13] as well as hydrophobicity of the CNT walls.[14] Here, in addition to simulations in periodic channels, we perform simulations of water flow in double-walled carbon nanotubes (DWCNT) embedded in heterogeneous membranes with thickness between 3 nm and 2000 nm. We demonstrate that, under the experimentally imposed pressures of the order of 1 bar, water entry into and exit from the CNT cavity is feasible only for pre-wetted membranes. We identify a significant pressure drop at the entrance and exit of the nanotube, leading us to reassess continuum models for water flow in CNTs. We explain why pressure losses must be accounted as end corrections in predicting such flow rates, and how disregarding such losses can lead to erroneous interpretations of the results.

The present results provide a thorough investigation of water transport in CNT membranes

and suggest that reported superfast water transport rates must be attributed to effects other than hydrodynamic interactions of water with a pure CNT interior.

We investigate water transport through CNT membranes (Figure 1) by distinguishing three successive stages of the entire process:

- water entry and filling of the CNT (Stage 1: Figure 1a).
- water emergence and droplet formation at the pore exit (Stage 2: Figure 1b).
- water flow through the CNT pore connecting two water reservoirs (Stage 3: Figure 1c).

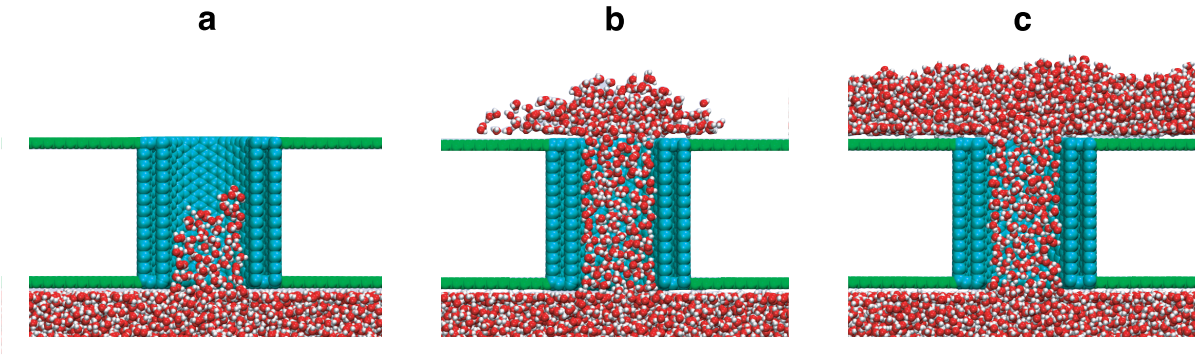

Figure 1: The three stages of simulated water transport through a DWCNT membrane: (a) Stage 1: Water entry (lower end) and filling of the nanotube with an external pressure ($P_{ext} > 120\,\mathrm{bar}$); (b) Stage 2: Emergence of water from the CNT exit ($P_{ext} > 1000\,\mathrm{bar}$) and formation of a nanodroplet at the low pressure side; (c) Stage 3: After the low pressure side is wetted, there is fast water transport through the membrane under reduced pressure. The figure shows a cut through the membrane with the hydrophobic DWCNT ($L = 3\,\mathrm{nm}, D = 2.034\,\mathrm{nm}$) (cyan), the hydrophilic membrane walls (green) on the high and low pressure sides, and the water molecules (red/white).

The investigated DWCNT has a chirality of $(15,15)$ for the inner CNT and $(21,21)$ for the outer CNT. These correspond to radii of $1.017\,\mathrm{nm}$ and $2.85\,\mathrm{nm}$ for the inner and the outer CNT, respectively. The lengths of the simulated CNTs (i.e. thicknesses of the embedding membranes) are in the range $1.4\,\mathrm{nm}$–$2\,\mu\mathrm{m}$. The lateral extent of each membrane wall is $18.17 \times 17.87\,\mathrm{nm}^2$ and the pore density of the membrane is $0.308 \times 10^{12}\,\mathrm{cm}^{-2}$. These values have been chosen near the experimentally investigated conditions of Holt et al.[3] We note that the membranes fabricated by Holt et al.[3] had an average pore radius of $0.8\,\mathrm{nm}$ and a thickness of $2\,\mu\mathrm{m}$, while the membrane

matrix was composed of silicon nitride, a hydrophilic material.[25] The present simulations are the first to emulate these flow conditions at μm thick membranes.

We use the SPC/E water model[26] using a smooth truncation at 1 nm of the electrostatic interactions[27] and a time step of $2fs$. The interaction between the water molecules and the carbon atoms are described by the Lennard-Jones (LJ) potential of Werder et al.[28] The membrane matrix is modeled as graphene with a hydrophilic water-carbon LJ interaction ($\sigma_{CO_m} = 0.319$ nm, $\varepsilon_{CO_m} = 0.5925\,\mathrm{kJ\,mol^{-1}}$, which correspond to a contact angle of 47° for water droplets on silicon nitride[28]).

In all cases, a 7.2 nm-thick slab of water is placed on the high pressure side (lower side in Figure 1) of the membrane. Water is driven into the CNT by a rigid graphene layer acting as a piston that applies constant pressure. Simulations were performed with two different codes, FASTTUBE[29] and NAMD.[30] The parallel capabilities of NAMD enabled the first ever molecular simulation of 2 μm long CNTs.

For the hydrophobic CNT walls ($\sigma_{CO} = 0.319$ nm, $\varepsilon_{CO} = 0.392\,\mathrm{kJ\,mol^{-1}}$, corresponding to $\theta = 95°$ cf. Ref.[28]), we find that, as expected, water molecules do not readily enter the CNT cavity unless significant external pressure is applied on the water slab. On the other hand, water molecules readily enter the CNT when the hydrophobicity of the CNT is reduced (maintain value of σ_{CO} with $\varepsilon_{CO} = 0.422\,\mathrm{kJ\,mol^{-1}}$, for which $\theta = 87°$). Furthermore, we find that a nominally hydrophobic CNT with a radius of 0.4 nm gets filled by a single water filament with zero applied pressure, consistent with results reported in previous simulations.[5,6,31] These tests with varying CNT diameters indicate that while sub-nm diameter hydrophobic CNTs get filled with water even in the absence of external pressure, 2-nm diameter CNTs resist filling, as one would expect at the macroscale.

We investigate first the filling process of the hydrophobic 1.017 nm-radius CNT by varying the pressure exerted by the piston onto the water slab at the entrance of the membrane and find that no water enters the CNTs for pressure differences below 100 bar. This value is consistent with the estimate obtained from the continuum Young-Laplace equation, shown to be valid at the nanoscale

regime[32]

$$\Delta P_{YL} = \frac{2\gamma}{r} = 2\gamma\frac{\cos\theta}{R}, \tag{1}$$

where ΔP_{YL} is the Young-Laplace pressure across the meniscus, γ the water surface tension, and r the radius of curvature of the meniscus within the CNT. Assuming a meniscus in the shape of a semi-spherical cap, we infer $r = R/\cos\theta$ with θ denoting the water contact angle and R the CNT radius. With a water surface tension $\gamma = 72\,\mathrm{mN\,m^{-1}}$ and a contact angle $\theta = 95^\circ$, the Young-Laplace pressure is 121 bar. When pressures (ΔP) above 121 bar are exerted water enters and fills the CNT.

In Figure 2 we compare, the observed volumetric CNT filling rates with the penetration rates $Q(t)$, for a column of fluid of length $l(t)$ advancing in a capillary (with slip length L_s), subject to entrance losses ($\mu CQ/R^3$; C is the loss coefficient),[33] and opposed by the Young-Laplace pressure of the non-wetting meniscus:[34,35]

$$\Delta P = \frac{\mu CQ}{R^3} + \frac{8\mu l(t)Q}{\pi(R^4 + 4R^3L_s)} - \frac{2\gamma\cos\theta}{R}, \tag{2}$$

Here $\mu = 0.91 \times 10^{-3}\,\mathrm{Ns/m^2}$ is the dynamic viscosity for SPC/E water. Figure 2 shows that Eq. (2), evaluated at $l(t) = L$, is in good agreement with the MD results by fitting the data with $L_s = 63\,\mathrm{nm}$ and $C = 1.77 \pm 0.25$. These values were selected as optimal for fitting the MD data using Eq. (2). The magnitude of the slip length is consistent with the slip $L_s = 72\,\mathrm{nm}$ reported for periodic systems,[9] and the value $63 \pm 4\,\mathrm{nm}$ reported in a recent extensive study[15] of water flow in channels with planar walls. Moreover, the above value of C is in good agreement with the single entrance loss coefficient $C = 1.5$ predicted for continuum, low Reynolds number flow[36] . We note that if the entrance losses are excluded from this analysis ($C = 0$), one incorrectly deduces slip lengths that vary with the length of the CNT, namely $L_s = 1.1\,\mathrm{nm}$, $1.4\,\mathrm{nm}$ and $3.6\,\mathrm{nm}$, for the corresponding CNT lengths of 3 nm, 6 nm and 12 nm. Thus, we find that the entrance losses dominate the flow in short CNTs. In fact, for the 3 nm-long CNT the entrance losses constitute 98 % of the total pressure loss.

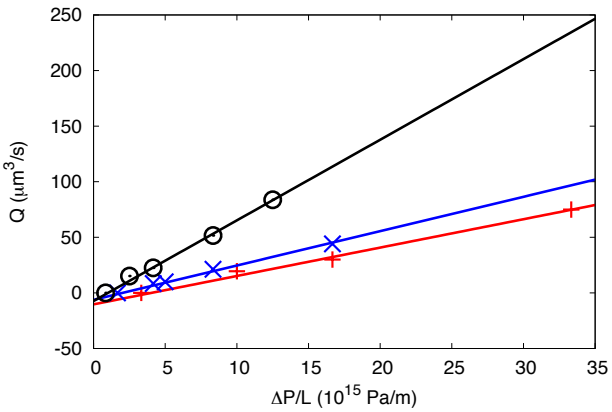

Figure 2: Volumetric flow rate (Q) versus pressure gradient ($\Delta P/L$) along the CNT in Stage 1 (filling) for different lengths (L) of the CNT: 3 nm:+; 6 nm:×; 12 nm:⊙. The lines correspond to regressions of Eq. (2) with the proper slip length (L_s) and entrance loss coefficient (C).

The present MD simulations indicated that water does not spontaneously enter hydrophobic CNTs with diameters above 1 nm. The formation of a water meniscus requires pressures in excess of the Young-Laplace value in order for water to enter the CNT. After water enters and gets transported through the CNT (Stage 1), it does not readily exit to the low pressure side of the CNT membrane. Similar to the situation during entrance flow, and as expected, a meniscus is formed at the exit of the CNT, resisting further water transport through the CNT. The simulations show that the minimum pressure required to force water out of the CNT is approximately 1000 bar. For higher pressures, a positive flow rate leads to the formation of a growing drop at the exit of the CNT and eventually to a continuous flow through the CNT membrane. These excessive pressures are consistent with the value (1035 bar) of the Young-Laplace pressure Eq. (1) for a water-filled CNT with a droplet just emerging at the low pressure side of the hydrophilic membrane with a contact angle of $\theta = 47^\circ$. The water volume at the CNT exit increases progressively, in turn increasing its radius of curvature and consequently lowering the pressure required to sustain the flow of new water molecules through the tube. It is envisioned that in practice, such high pressures may not be necessary due to prewetting of the membrane.

In Stage 3, the CNT has been filled along its entire length, and water exiting the CNT meets a nanometer thick water film. We vary the externally applied pressure in conjunction with the CNT

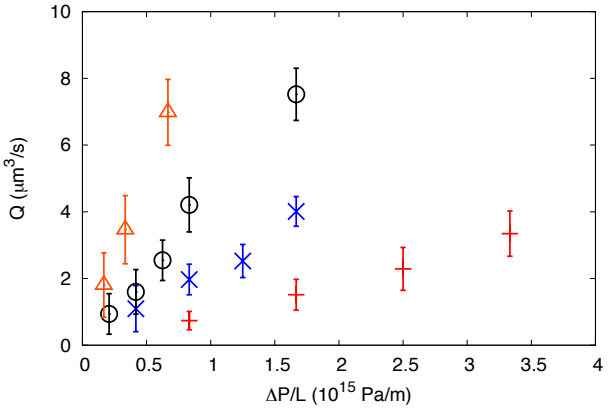

(a)

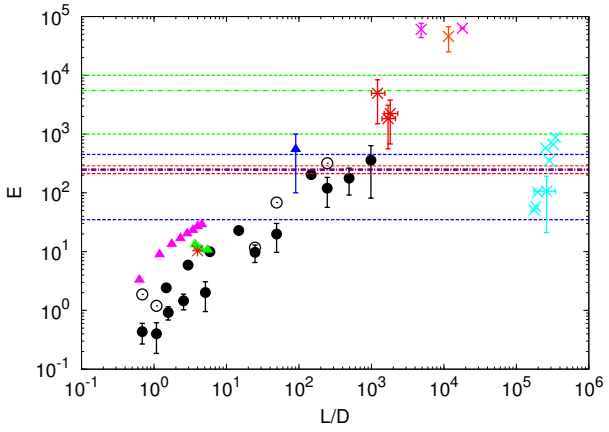

(b)

Figure 3: (a) Volumetric flow rate (Q) versus imposed pressure gradient ($\Delta P/L$) along the CNT for Stage 3 (continuous flow), as determined from the MD simulations: 3 nm: ⟝⟞; 6 nm: ⟝×⟞; 12 nm: ⟝○⟞; 30 nm: ⟝△⟞. The error bars show the standard error of the mean. (b) Enhancement dependence on the ratio of CNT length over diameter. For μm CNT lengths the enhancement rates observed for membranes asymptote to the results of periodic simulations and are in good agreement with experimental results.[4] In the figure *circles* correspond to present simulation results, *triangles* are other MD simulations and *crosses* are experimental results. *Dot-dashed* lines are results from MD simulations of periodic CNTs, and *dashed lines* denote their standard deviation. ● and ------ correspond to simulations using FASTTUBE.[29] ⟝●⟞ and ⊙ correspond to 200 and 20 *bar*, respectively, pressure bias using NAMD.[30] Error bars for 200 *bar* pressure represent ± half standard deviation. ⟝×⟞ , ⟝×⟞, ⟝×⟞ and × correspond to enhancement values reported by Holt,[3] Majumder[1,2] and Qin,[4] respectively. ⟝×⟞ correspond to enhancement values reported by Qin[4] using a reduced diameter in the calculation of the CNT area. ⟝▲⟞, ▲ and ▲ correspond to enhancement values reported by Thomas,[16] Wang[12] and Su.[11] ------, ------ and ------ correspond to enhancement values reported by Falk[14] and Thomas,[9,13] respectively. The, ✳ correspond to enhancement values for aquaporins as calculated using results from previous studies.[17,37,38]

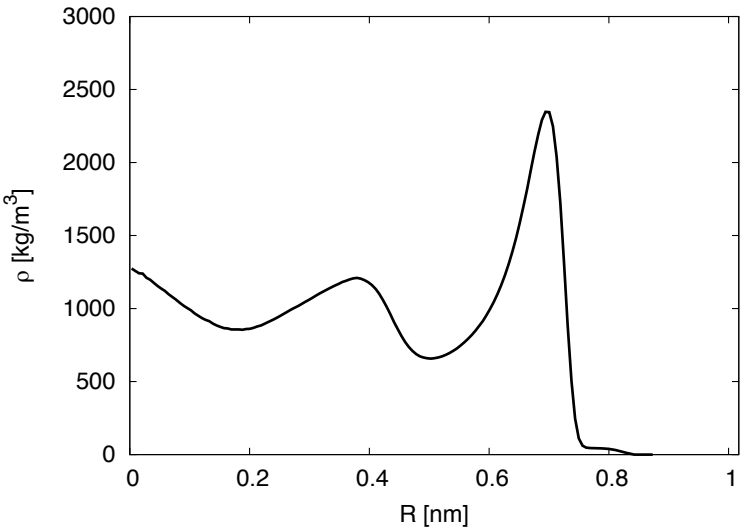

Figure 4: Averaged Radial Density Profile of Water inside the CNT in Stage 3, with 0, representing the centre of the CNT

length and in Figure 3a we plot the MD volumetric flow rates versus the imposed pressure gradient $\Delta P/L$. The water inside the CNT exhibits a layered structure (Figure 4), a representative behaviour of water confinement in CNTs[39] . The flow rate is observed to increase linearly with the imposed pressure gradient, contrary to the nonlinear dependence suggested by Thomas and McGaughey.[16]

In Figure 3b we present enhancement rates for different MD simulations and experiments, as well as the rates calculated for aquaporins. For μm length CNTs the enhancement rates observed for membranes asymptote to the results of periodic simulations and are in good agreement with experimental results[4].

To explore this outcome further, we consider the slip and entrance/exit loss modified Hagen-Poiseuille expression:[19,33]

$$\Delta P = \frac{\mu C Q}{R^3} + \frac{8\mu L Q}{\pi(R^4 + 4R^3 L_s)} \tag{3}$$

where the coefficient C represents the sum of both fluid entry and exit losses.

The corresponding, no-slip Hagen-Poiseuille flow rate Q^{HP} is $Q^{HP} = \frac{\pi R^4 \Delta P}{8\mu L}$, so that from Eq. (3) we deduce that the flow rate enhancement ratio $E = Q/Q^{HP}$ can be expressed as a simple

function of dimensions of the CNT, the slip length and the pressure entry/exit losses:

$$\frac{1}{E} = \frac{1}{1+4L_s/R} + \frac{C\pi R}{8}\frac{1}{L} \tag{4}$$

From Eq. (4) we remark that ignoring pressure and exit losses ($C = 0$) or for infinitely long CNTs, the enhancement is $E = Q/Q^{HP} = 1+4L_s/R$. Thus, based on continuum analysis, the enhancement ratio E can reach a maximum theoretical value of 253, based on $L_s = 63\,\text{nm}$, as determined for Stage 2. In all of the present simulations, the values of E remained below this theoretical limit (Figure 3b). The results suggests that entrance and exit effects can be ignored for CNT lengths above $\approx 300\,\text{nm}$. For shorter CNTs, the calculated values of E rise with CNT length. This trend is consistent with recent results[11] for water flow in sub-10 nm CNTs subjected to $\Delta P = 1800\,\text{bar}$ and 300 K, or[12] for CNT lengths 6–15 nm under $\Delta P = 50\,\text{bar}$ and 300 K. Both of these studies reported values of E in the range 10–30, which are near our values for the corresponding CNT lengths. On the other hand, although the rising E vs. L trend was also reported in[40] for CNT lengths up to 50 nm, $\Delta P = 2000\,\text{bar}$ and 298 K, the corresponding values of E therein exceeded 1500, thus being well above even the highest value we find for $2\,\mu\text{m}$ (Figure 3b) and the theoretical limit (253) for infinite length from Eq. (4).

We note that the contradictory transport rates reported in the MD simulations may also be attributed to the different ways of estimating them. For example, in[9,13] as well as in the present work, transport rates are calculated by measuring the net number of molecules that exit the CNT. In[14] these rates are extrapolated by calculating molecular friction coefficients and estimating the corresponding transport rates from continuum approximations. We consider that for *nm* diameters, these extrapolations to the continuum may not be valid, as the local density and viscosity of the fluid (Figure 4) is varying significantly across the CNT. Finally, in some MD simulations the full CNT cross-section is considered as the effective transport area, while in others this is calculated using a reduced (by $1\sigma_{CO}$) CNT radius. This difference affects the measured transport rates as reported in[4] and is shown in Figure 3b.

In summary, for shorter CNTs the observed length dependence of E is attributed to entrance and exit losses, whereas the asymptotic value for long CNTs is governed solely by the slip length. We itertate that the present MD results are the first to be performed at micrometer long CNTs, thus eliminating questions associated with the validity of periodic simulations and are consistent with continuum analysis accounting for slip and entry/exit losses. The results suggest that the anomalously high flow enhancement rates reported in previous experimental and MD studies cannot be attributed to interactions of water with pristine CNTs. This insight can assist further experimental and computational studies leading to rational design of CNT membranes for super fast water transport. Ongoing research in our group aims at a systematic Uncertainty Quantification study of the results of the MD simulations [18] and QM/MM simulations so as to quantify the role of the various simulation parameters on the predicted transport rates. Further work includes simulations that aim to identify alternative mechanisms responsible for the observed rates, such as modification of the hydrophilic entrance [1,41] and/or doping of the CNT walls, that may be responsible for the reported high transport rates.

Acknowledgement

This material is based upon work supported in part by the US National Science Foundation under Grant NIRT CBET 0609062. Computer time was provided by the Swiss National Supercomputing Center (CSCS).

References

(1) Majumder, M.; Chopra, N.; Andrews, R.; Hinds, B. J. *Nature* **2005**, *438*, 44.

(2) Majumder, M.; Chopra, N.; Hinds, B. J. *ACS NANO* **2011**, *5*, 3867–3877.

(3) Holt, J. K.; Park, H. Y.; Wang, Y.; Stadermann, M.; Artyukhin, A. B.; Grigoropoulos, C. P.; Noy, A.; Bakajin, O. *Science* **2006**, *321*, 1034 – 1037.

(4) Qin, X.; Yuan, Q.; Zhao, Y.; Xie, S.; Liu, Z. *Nano Lett.* **2011**, *11*, 2173–2177.

(5) Hummer, G.; Maxwell, J. C.; Noworyta, J. P. *Nature* **2001**, *414*, 188 – 190.

(6) Waghe, A.; Rasaiah, J. C.; Hummer, G. *J. Chem. Phys.* **2002**, *117*, 10789 – 10795.

(7) Kalra, A.; Garde, S.; Hummer, G. *Proc. Natl. Acad. Sc. USA* **2003**, *100*, 10175 – 10180.

(8) Corry, B. *J. Phys. Chem. B* **2008**, *112*, 1427–1434.

(9) Thomas, J. A.; McGaughey, A. J. H.; Kuter-Arnebeck, O. *Internat. J. Thermal Sci.* **2010**, *49*, 281 – 289.

(10) Suk, M. E.; Aluru, N. R. *J. of Phys. Chem. Lett.* **2010**, *1*, 1590–1594.

(11) Su, J.; Guo, H. *J. Phys. Chem. B* **2012**, *116*, 5925–5932.

(12) Wang, L.; Dumont, R. S.; Dickson, J. M. *J. Chem. Physics* **2012**, *137*, 044102.

(13) Thomas, J. A.; McGaughey, A. J. H. *J. Chem. Phys.* **2008**, *128*, 084715.

(14) Falk, K.; Sedlmeier, F.; Joly, L.; Netz, R. R.; Bocquet, L. *Nano Lett.* **2010**, *10*, 4067–4073.

(15) Kannam, S. K.; Todd, B. D.; Hansen, J. S.; Daivis, P. J. *J. Chem. Phys.* **2012**, *136*, 024705.

(16) Thomas, J. A.; McGaughey, A. J. H. *Phys. Rev. Lett.* **2009**, *102*, 184502.

(17) Zhu, F.; Tajkhorshid, E.; Schulten, K. *Biophys. J.* **2002**, *83*, 154–160.

(18) Angelikopoulos, P.; Papadimitriou, C.; Koumoutsakos, P. *J. Chem. Phys.* **2012**, *137*, 144103.

(19) Sisan, T. B.; Lichter, S. *Microfluid. Nanofluid.* **2011**, *11*, 787–791.

(20) Zhu, Y.; Granick, S. *Phys. Rev. Lett.* **2002**, *88*, 106102–1–106102–4.

(21) Sokhan, V. P.; Nicholson, D.; Quirke, N. *J. Chem. Phys.* **2002**, *117*, 8531–8539.

(22) Whitby, M.; Quirke, N. *Nature Nanotechnol.* **2007**, *2*, 87–94.

(23) Goldsmith, J.; Martens, C. C. *Phys. Chem. Chem. Phys.* **2009**, *11*, 528–533.

(24) Myers, T. G. *Microfluid. Nanofluid.* **2011**, *10*, 1141–1145.

(25) Saadaoui, M.; Wien, W.; van Zeijl, H.; van den Bogaard A.,; Sarro, P. M. *Proc. SAFE & ProRISC 2004* **2007**, 543–546.

(26) Berendsen, H. J. C.; Grigera, J. R.; Straatsma, T. P. *J. Phys. Chem.* **1987**, *91*, 6269 – 6271.

(27) Levitt, M.; Hirshberg, M.; Laidig, K. E.; Daggett, V. *J. Phys. Chem. B* **1997**, *101*, 5051–5061.

(28) Werder, T.; Walther, J. H.; Jaffe, R. L.; Halicioglu, T.; Koumoutsakos, P. *J. Phys. Chem. B* **2003**, *107*, 1345 – 1352.

(29) Walther, J. H.; Jaffe, R. L.; Halicioglu, T.; Koumoutsakos, P. *J. Phys. Chem. B* **2001**, *105*, 9980 – 9987.

(30) Phillips, J. C.; Braun, R.; Wang, W.; Gumbart, J.; Tajkhorshid, E.; Villa, E.; Chipot, C.; Skeel, R. D.; Kale, L.; Schulten, K. *J. Comput. Chem.* **2005**, *26*, 1781–1802.

(31) Zimmerli, U.; Walther, J. H.; Koumoutsakos, P. *Nano Lett.* **2005**, *5*, 1017 – 1022.

(32) Thompson, P.; Brinckerhoff, W.; Robbins, M. *J. Adhesion Sci. Tech.* **1993**, *7*, 535–554.

(33) Weissberg, H. L. *Phys. Fluids* **1962**, *5*, 1033–1036.

(34) Lucas, R. *Kolloid-Zeitschrift* **1918**, *23*, 15–22.

(35) Washburn, E. W. *Phys. Rev.* **1921**, *17*, 273 – 283.

(36) Sisavath, S.; Jing, X.; Pain, C. C.; Zimmerman, R. W. *J. Fluids Engng.* **2002**, *124*, 273–278.

(37) Walz, T.; Smith, B. L.; Zeidel, M. L.; Engel, A.; Agre, P. *J. Biol. Chem.* **1994**, *269*, 1583–1586.

(38) Wang, Y.; Schulten, K.; Tajkhorshid, E. *Structure* **2005**, *13*, 1107–1118.

(39) Joseph, S.; Aluru, N. R. *Nano Lett.* **2008**, *8*, 452–458.

(40) Nicholls, W. D.; Borg, M. K.; Lockerby, D. A.; Reese, J. M. *Microfluid. Nanofluid.* **2012**, *12*, 257–264.

(41) Fornasiero, F.; Park, H. G.; Holt, J. K.; Stadermann, M.; Grigoropoulos, C. P.; Noy, A.; Bakajin, O. *Proc. Natl. Acad. Sc. USA* **2008**, *105*, 17250–17255.